

Structural Nonlinearities and their Impact on the Fidelity of Critical Steady Maneuver Loads and Trimming Configuration of Very Flexible Airframes

(Received: December 24, 2017. Revised: June 13, 2018. Accepted: July 20, 2018)

M. A. A. SALMAN¹
MOSTAFA S. A. ELSAYED²
DENIS WALCH³

Abstract

The intensive design optimization of airframes has the effect of decreasing the structural stiffness, which can induce large deformations. Such changes can have a significant effect on the flight loads as well as the trimming configuration of the aircraft. Iterative solutions to approach this problem have been proposed in literature, coupling nonlinear structural solution methods with linear aerodynamics. In this paper, a modified iterative methodology is proposed, which includes the downwash effect of the aerodynamic twist into the solution sequence to improve the fidelity of the calculated aerodynamic loads compared to the existing method. A case study is presented to investigate the differences in the wing loads of interest and trimming configuration when the effect of geometric nonlinearities are included in the static aeroelastic analysis, as the mass and stiffness is varied. Increases of 20%, 13% and 30% are observed in the out of plane bending moment, out of plane shear force and torque for the most flexible variant of the airframe considered. Additionally, significant differences are observed in the corresponding trimming configuration, with changes of -12% and -8% in the trimmed angle of attack and elevator deflection respectively.

1 Introduction

Minimizing aircraft weight to maximize its fuel efficiency is among the major design objectives in new aircraft development programs [18]. The general trend towards increasing the fuel efficiency of the aircraft has led to the shift towards higher aspect ratio wings due to the significant effect on induced drag [4]. As induced drag is a very significant part of total drag, reducing it can have significant effects on fuel economy [1]. Both of these design trends have the effect of increasing the deformation of the aircraft wing under loading. Weight minimization leads to reduced torsional and bending stiffness, which in turn lead to increased wing deflections under load. Similarly increasing the aspect ratio leads to a more slender wing, which increases the wing deflection. However, the slenderness and reduced overall stiffness of high aspect ratio wings lead to higher deflections, resulting in nonlinear behaviour. Such nonlinear effects can have a significant effect on the aeroelastic behaviour of the aircraft, which has been covered by a number of survey and review papers [44, 2].

An unintended consequence of such behavior is that it moves away from what is expected from the typical linear structural model. As such, geometrically nonlinear effects have to be taken into account during the design process especially in the aeroelastic analysis of the aircraft, to better model its performance under large deformations and as such, need to be included in any high fidelity aeroelastic solution sequence [25].

¹ Graduate Student, Carleton University
Ottawa, Ontario K1S 5B6, Canada

² Professor of Aerospace Engineering
Ottawa, Ontario K1S 5B6, Canada

³ Engineering Specialist, Bombardier Aerospace
St-Laurent, QC, H4S 1Y9, Canada

The most commonly used formulation for modeling the effects of geometric nonlinearities in structural analysis is the displacement based method (also known as stiffness formulations method). Here, the nonlinear formulation for twisted and curved beams, such as nonlinear composite beam theory by Bauchau and Hong, is one such implementation [6, 7]. Since the independent variables are the rotation and displacement, visualization and application of the constraints is straight forward. However, the presence of higher order nonlinear terms in the deformation field makes the displacement-based formulations computationally expensive [40]. It should be noted that this methodology is the most commonly used in commercial finite element codes.

Another formulation for modeling nonlinearities is the intrinsic formulation, based on the foundation for the nonlinear exact equilibrium equations for thin beams under deformation, given in Loves Treatise on the Mathematical Theory of Elasticity [28]. The original formulation considered bending and rotation and extension of the beam, and was expanded upon by Reissner [34] to include transverse force and deformation. The work done by Hegemier and Nair [20] continued the work of Reissner, to formulate large deformations - small strain theory for untwisted isotropic rods in extension, bending and twist. The formulation consisted of equations of motion and kinematical formulae with unknowns including stress resultants, generalized strains and velocities [23]. Hodges built upon this approach by completing the geometrically exact intrinsic nonlinear formulation for a curved and twisted moving anisotropic beams [22]. In his formulation, the governing equations did not contain displacement and rotation variables, eliminating singularities associated with finite rotation variables [23]. This led to the formulation having a nonlinearity with a maximum order of two, simplifying calculations and reducing computational cost [22, 44]. In addition, mixed variational formulations potentially can have higher solution accuracy and robustness than displacement based formulations [48]. For structures that are better represented as plates than beams, a formulation for moving anisotropic plates is presented by Hodges, et.al. [24].

Strain based formulations represent the beam deformation with strain, twist, and curvature as the independent degrees of freedom [16]. One of the advantages of strain based formulations in a finite element simulation is to avoid the shear locking phenomenon and accurate representation of rigid body modes [36]. Forces and moments within the beam can be directly obtained from the respective strains without additional differentiation of displacement variables, while maintaining the same level of accuracy as obtained for the strains [49]. Su and Cesnik presented a strain based formulation that iteratively solve the beam equilibrium and strain displacement equations, simplifying the solution process, allowing for more flexibility in arbitrary loading and beam displacement configurations [40].

The study of aeroelasticity of highly flexible aircraft configurations has been investigated using a large range of methods. Modal methods were used to calculate the loads on a High Altitude Long Endurance type aircraft by using selected vibration and rigid body modes of the aircraft [42]. However, this analysis did not consider the effects of large deformation geometrical nonlinearities. Their effect on the flutter performance of aircraft was investigated by Patil et al., using a nonlinear mixed variational formulation based on the work done by Hodges et. al [24, 21]. Significant differences were found in flutter speed when compared to existing linear methods [32]. Tang and Dowell used the nonlinear beam model by Hodges and Dowell with the ONERA nonlinear stall model [29] to investigate Limit Cycle Oscillations (LCO) and flutter effects [41]. Xie et. al conducted a geometrically nonlinear analysis of a wing, using MSC Nastran to obtain the natural frequency and mode shapes of the structure. The aeroelastic analysis performed indicated that nonlinear effects play a significant role in highly flexible wings [45, 46]. High fidelity geometrically nonlinear three-dimensional finite element modes, coupled with computational fluid dynamics analysis were

used by Garcia to investigate the effects of geometric nonlinearities on the twist distribution along the wing, in static aeroelastic maneuvers. Nonlinear bending-torsion coupling was shown to affect the twist, leading to control reversal in the nonlinear case [17]. Strain based geometrically nonlinear models, coupled with unsteady aerodynamics, and were used to investigate the flight dynamics of a HALE type aircraft under various flight conditions, including ascent, descent, and control surface inputs. The effects of nonlinearities were shown to be significant during asymmetric maneuvers, and when the mass of the aircraft was increased [38]. Further work has been performed in the field of nonlinear structural aeroelasticity, studying the effect nonlinearities have on different aircraft configurations, such as joined-wing and flying-wing configurations [27, 33, 31].

In this paper, the theory behind the nonlinear iterative methodology will be presented in the next section. Following that, the implementation of the theoretical methodology will be explained, along with the details of the case study, and the beam parametrization being used. The results will be split into three sections, the first being the improvements obtained when using the modified nonlinear methodology on the relatively stiff baseline aircraft structure. The second section will present the results of the study into the effect of nonlinearities at higher wing root angles. The final section will investigate the importance of having a nonlinear aeroelastic solution when the aircraft structural parameters are modified, as often is done during a multidisciplinary optimization.

2 Theoretical Background

21 Nonlinear Structural Formulation

In linear structural analyses, equations of equilibrium are formulated with respect to undeformed geometry as geometrical variations due to infinitesimal deformations are negligible [10]. However, when the deformations are unbounded, they become large enough to develop considerable geometrical changes and the equilibrium equations are formulated with respect to the deformed structure, resulting in nonlinear governing equations of motion [37].

Commercial Finite Element code packages, such as MSC Nastran [26], often use a Lagrangian method, where the Finite Element mesh follows the deformation of the structure [8]. Within this, there are two formulations, the Total Lagrangian Formulation (TLF) [30] and the Updated Lagrangian Formulation (ULF) [5]. In the TLF, equilibrium is expressed relative to the original undeformed structure, while in the ULF, the reference state is the current [5].

We adopt in this paper the ULF nonlinear finite element approach [5]. Here, equations of motion are formulated with respect to the state of the structure at time $t + \Delta t$, where Δt is the time from the previous to the current load iteration. Following the principle of virtual work, the methodology is formulated as follows.

The external virtual work, ${}^{t+\Delta t}W$, of a deformed system at time $t + \Delta t$ can be expressed in terms of the 2nd Piola-Kirchoff stress tensor, ${}^{t+\Delta t}S_{ij}$, and a variation in the Green-Lagrange strain tensor, ${}^{t+\Delta t}\delta\varepsilon_{ij}$, with respect to the configuration at time t , as:

$$\int_V ({}^{t+\Delta t}S_{ij}) ({}^{t+\Delta t}\delta\varepsilon_{ij}) dV = {}^{t+\Delta t}W \quad (1)$$

where $i, j \in \{1, 2, 3\}$. The Green-Lagrange strain tensor and the 2nd Piola-Kirchoff stress tensor are given by:

$${}^t\varepsilon_{ij} = {}^te_{ij} + {}^t\eta_{ij} \quad (2)$$

$${}^tS_{ij} = {}^tC_{ijrs} {}^t\varepsilon_{rs} \quad (3)$$

where ${}^te_{ij}$ and ${}^t\eta_{ij}$ are the linear and nonlinear strain components, respectively. ${}^tC_{ijrs}$ are the components of the elasticity tensor, and $r, s \in \{1, 2, 3\}$. At the

incremental time step $t + \Delta t$, the stress tensor is expressed as:

$${}^{t+\Delta t}S_{ij} = {}^tS_{ij} + {}^t\tau_{ij} \quad (4)$$

where ${}^t\tau_{ij}$ are components of the Cauchy stress. Substituting Eqs. 2, 3 and 4 into Eqn. 1, the finite element formulation of the equation of motion can be expressed as:

$$\begin{bmatrix} {}^t\mathbf{K}^L & + & {}^t\mathbf{K}^G \\ \text{linear} & & \text{nonlinear} \end{bmatrix} \mathbf{u} = {}^{t+\Delta t}\mathbf{R} - {}^t\mathbf{F} \quad (5)$$

where \mathbf{u} is the vector of displacements between time t to $t + \Delta t$, ${}^{t+\Delta t}\mathbf{R}$ is the finite element evaluation of Eqn. 1, and ${}^t\mathbf{F}$ is the external work. The material stiffness matrix is given by:

$${}^t\mathbf{K}^L = \int_V [{}^t\mathbf{B}^L]^T {}^t\mathbf{C} [{}^t\mathbf{B}^L] dV \quad (6)$$

the nonlinear geometric stiffness matrix is given by:

$${}^t\mathbf{K}^G = \int_V [{}^t\mathbf{B}^G]^T {}^t\boldsymbol{\tau} [{}^t\mathbf{B}^G] dV \quad (7)$$

and the external work is given by:

$${}^t\mathbf{F} = \int_V [{}^t\mathbf{B}^L]^T {}^t\hat{\boldsymbol{\tau}} dV \quad (8)$$

where \mathbf{B}^L and \mathbf{B}^G are the corresponding strain-displacement transformation matrices, ${}^t\boldsymbol{\tau}$ and ${}^t\hat{\boldsymbol{\tau}}$ are the matrix and vector of Cauchy stresses at time t , respectively. The two stiffness matrices are assembled for the current state at time $t + \Delta t$, and the nonlinear terms arise from the quadratic terms in Equation 2.

In a standard linear aeroelastic analysis, the aerodynamic pressure, \hat{f} , is expressed as:

$$\hat{f} = q\mathbf{A}^{-1}\hat{w} \quad (9)$$

where the downwash, \hat{w} , is given by:

$$\hat{w} = \mathbf{D}\hat{u} + \hat{w}^g \quad (10)$$

The Aerodynamic Influence Coefficient (AIC) matrix is given by \mathbf{A} , q is the dynamic pressure at the desired flight conditions, and \mathbf{D} is the matrix relating the displacements of the aerodynamic panels, \hat{u} , to the downwash. For a standard linear solution, the additional downwash vector \hat{w}^g is usually zero, unless the wing being modeled has an initial camber or a twist distribution. The additional downwash vector is used to include the nonlinear component of the wing twist due to large deformation effects.

The total aerodynamic force on the structure, \hat{L} , can then be expressed as:

$$\hat{L} = \mathbf{S}\hat{f} + \hat{P} \quad (11)$$

where \hat{P} is a vector of rigid applied loads on the structure such as engine loads and point loads, and \mathbf{S} is a matrix relating the nodal pressures to nodal forces.

The force and displacement relationship for a static structural problem, in general, can be expressed as:

$$\hat{F} = \mathbf{K}\hat{u} \quad (12)$$

where \hat{F} is the elastic force due to deformation \hat{u} . The stiffness matrix, \mathbf{K} , is constant in the linear case, or a function of displacement in the geometrically nonlinear case. When the aeroelastic system is at equilibrium, the entire system can be expressed as:

$$\mathbf{S}\hat{f} + \hat{P} = \mathbf{K}\hat{u} \quad (13)$$

Substituting in Eqns. 9 and 10 in Eqn. 13 results in a system of matrix equations that can be solved to obtain the final deformed configuration of the aircraft.

$$\mathbf{qSA}^{-1} [\mathbf{D}\hat{u} + \hat{w}^g] + \hat{P} = \mathbf{K}\hat{u} \quad (14)$$

To include the effects of geometric nonlinearity, an iterative method is used to update the vector of displacements, \hat{u} , and the updated stiffness matrix, which consists of a linear and geometrically nonlinear component, given by:

$$\mathbf{K} = \mathbf{K}^L + \mathbf{K}^G \quad (15)$$

The stiffness matrices are obtained using Eqns. 6 and 7, for the converged nonlinear structural problem. Equation 14 can be rewritten as:

$$\mathbf{Q}[\mathbf{D}\hat{u} + \hat{w}^g] + \hat{P} = [\mathbf{K}^L + \mathbf{K}^G] \hat{u} \quad (16)$$

where \mathbf{Q} is a matrix relating the nodal downwash to nodal forces. Equation 16 is solved using an iterative process, which results in the following relationship, where n is the iteration number.

$${}^n\mathbf{Q} [{}^n\mathbf{D} {}^n\hat{u} + {}^n\hat{w}^g] + {}^n\hat{P} = \underbrace{[{}^{n+1}\mathbf{K}^L]}_{\text{linear loads}} {}^{n+1}\hat{u} + \underbrace{[{}^{n+1}\mathbf{K}^G]}_{\text{nonlinear increment}} {}^{n+1}\hat{u} \quad (17)$$

Convergence criteria is determined by the difference in nodal displacement, u_k , with respect to the previous iteration, for all nodes along the wing, 1..k, given by:

$${}^n\sigma_e > \max ({}^{n+1}u_k - {}^nu_k) \quad (18)$$

Equation 17 is incremented until convergence; i.e. ${}^n\sigma_e$ is small. For the case study, the chosen convergence criteria is 0.1% difference in displacement between iterations. The increase in loads due to the inclusion of geometric nonlinearities can then be written as

$$\Delta_e = \left(\frac{[{}^n\mathbf{K}^L + {}^n\mathbf{K}^G] {}^n\hat{u}^{NL}}{{}^n\mathbf{K}^L \hat{u}^L} - 1 \right) \times 100\% \quad (19)$$

where \hat{u}^L and \hat{u}^{NL} are the linear and nonlinear deformed configuration of the aircraft.

22 Aerodynamic Formulation

The aerodynamic loads are calculated using Nastran SOL 144, which uses the Doublet Lattice Method [3]. This method is based on linearized potential flow theory, where a line of potential doublets of unknown strength lie on the quarter-chord of each panel. Given n 'boxes', with a constant force per unit length of the quarter-chord line, f , the strength of doublet line segment j is given by

$$\frac{f_j}{4\pi\rho} \int l_j ds \quad (20)$$

where l_j is the length of the doublet line, ds is an increment along the line, and ρ is the density of the air. The total downwash at any point on the aerodynamic surface, x_i, s_i , can then be written as the sum of all the downwashes due to the n doublets on the surface as follows

$$\bar{w}(x_i, s_i) = \sum_{j=1}^n \left(\frac{f_j}{4\pi\rho} U^2 \right) \int \hat{K} ds \quad (21)$$

where U is the freestream velocity, and \hat{K} is the kernel function for a nonplanar surface [43]. When Equation 21 is applied on all the downwash points, the force

per unit length along the quarter-chords of the boxes can be determined, and thus, the average pressure, \bar{P}_i , on each box can be written as

$$\bar{P}_i = \frac{f_i}{\Delta x_j \cos \lambda_j} \quad (22)$$

where Δx_j is the average chord of the j th box, and λ_j is the sweep angle of the doublet line on the box. Given j th index of doublet lines and i th index of the downwash points, Equation 21 can be re-written as

$$\bar{w}_i = \sum_{j=1}^n D_{ij} p_j \quad (23)$$

where D_{ij} are the elements of a matrix relating the aerodynamic pressures to the downwash at each point, given as follows

$$D_{ij} = \frac{\pi}{8} \Delta x_j \cos \lambda_j \int \hat{K} ds \quad (24)$$

Equation 10 represents the downwash acting on an aerodynamic panel. However, trimming the aircraft into a steady state condition often requires the use of aerodynamic degrees of freedom, such as angle of attack, rotation rates, and control surface deflections, to modify the net forces and moments acting on the structure, which can be incorporated into the expression for the downwash as follows:

$$\hat{w} = \mathbf{D}\hat{u} + \mathbf{D}_\sigma \hat{u}_\sigma + \hat{w}^g \quad (25)$$

where \mathbf{D}_σ is a matrix relating the aerodynamic degrees of freedom, \hat{u}_σ , to the downwash.

All prior equations assume that the aerodynamic forces are applied directly to the structural nodes. However, this is not always the case, as the aerodynamic loads are applied at the quarter-chord point of each aerodynamic box element, which may be much larger in number than the actual structural elements. The forces need to be coupled to the structural degrees of freedom of the airframe, which is achieved by the use of a linear beam spline. \mathbf{G} is an interpolation matrix relates the structural deflections \hat{u} to the aerodynamic grid point deflections, \hat{u}_k .

$$\hat{u}_k = \mathbf{G}\hat{u} \quad (26)$$

Imposing the condition that the virtual work performed by both deflections is identical, an expression for an arbitrary force transformation between the aerodynamic and structural nodes can be obtained:

$$\hat{F}_g = \mathbf{G}^T \hat{F}_k \quad (27)$$

where \hat{F}_k is a vector of aerodynamic loads, and \hat{F}_g are the corresponding loads on the structural nodes. The system of equations representing a linear static aeroelastic problem can then be expressed as follows:

$$[\mathbf{K}^L - \mathbf{QD}] \hat{u} + \mathbf{M}\ddot{\hat{u}} = \mathbf{Q}_\sigma \mathbf{D}_\sigma \hat{u}_\sigma + \hat{P} + \mathbf{Q}\hat{w}_g \quad (28)$$

This is similar to Equation 16, where \mathbf{Q}_σ relates the downwash due to a unit displacement of aerodynamic degrees of freedom (control surface deflections, incidence angles, rotation rates) to the aerodynamic forces, \mathbf{M} is the structural mass matrix, and $\ddot{\hat{u}}$ is a vector of rigid body accelerations. Given the free rigid body degrees of freedom, necessary constraints to other aerodynamic degrees of freedom, as well as the definition of the control surfaces, Equation 28 is partitioned into restrained and free degrees of freedom, and is solved to obtain the trimmed flight condition of the aircraft [35].

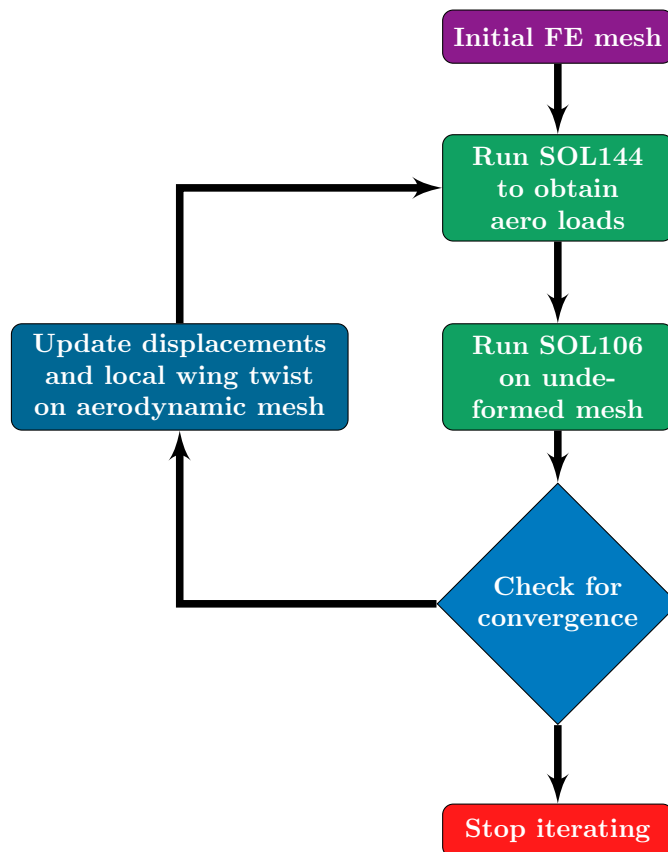


Figure 1: Flowchart depicting the Nastran Iterative Method

3 Methodology

This section outlines the developed methodology to couple linear aerodynamics to a nonlinear structural methodology to create an iterative solution which incorporates geometrically nonlinear effects into static aeroelasticity. In this paper, MSC Nastran is used for this purpose.

3.1 Modified Iterative Method

Equation 17 is implemented using the linear aeroelasticity and nonlinear structural analysis codes of MSC Nastran. In the flexible aeroelastic trim, the Doublet Lattice Method is used to calculate the aerodynamic loads on the aircraft, and update the deformed shape of the lifting surfaces based on linear structural mechanics. However, there is no nonlinear aeroelastic module present by default in Nastran. As such, a modified method, based on the iterative method proposed by [25], is used to determine the effects of large displacement nonlinearities on the aircraft loads. A flowchart of the overall process used in the iterative loop is shown in Figure 1.

This method uses linear panel method aerodynamics to calculate the loads on the structure, which are applied on the undeformed structure. A displacement based geometrically nonlinear method is used to calculate the nonlinear deformation of the structure, including follower force effects, and the new displacements are used to update the structural and aerodynamic mesh used for the aerodynamic loads calculation to obtain a new set of loads. The process is repeated until the structure converges at a deformed shape configuration. The loads acting on the aircraft due to its new deformed configuration can be obtained.

The aerodynamic implementation uses the doublet lattice method, which divides the surface into a number of panels, parallel to the free stream velocity [3]. However, the DLM implementation in Nastran places the flow direction in the

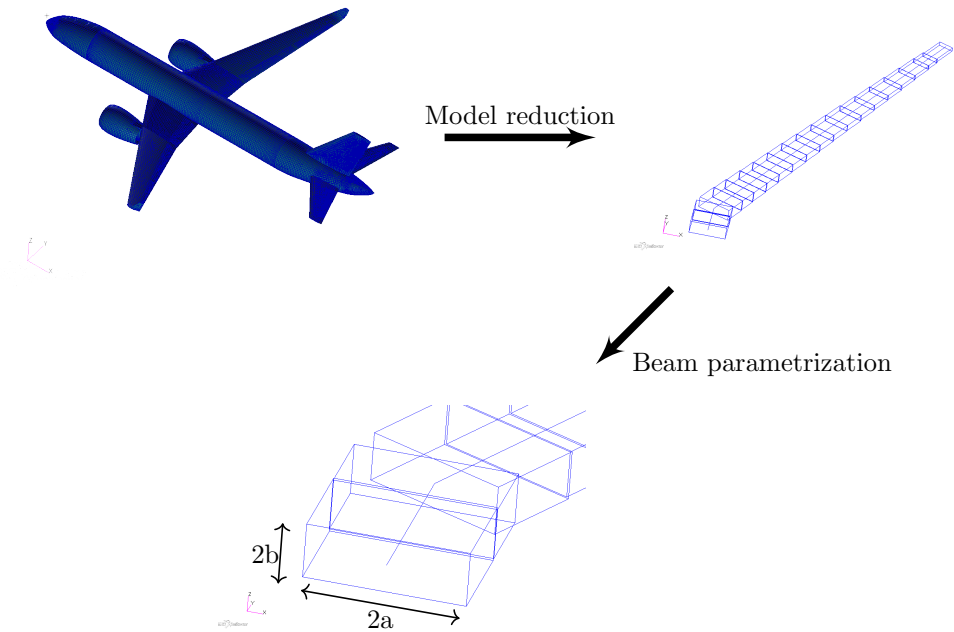


Figure 2: Reduction from Global Finite Element Model to Stick Model for a generic twin engine aircraft

positive x-direction, which has to be parallel to the x-axis of every aerodynamic element [35]. In addition, the resultant aerodynamic forces are applied in the coordinate system of the undeformed aerodynamic panel, which can lead to the aerodynamic forces having no inboard component, even under large deflections.

As the structure is assumed to be flexible, the effects of twisting along the wing on the generated lift cannot be ignored. As such, the first limitation can be resolved by implementing a downwash angle of attack on the aerodynamic panels corresponding to the local angle of attack along the wing. The second limitation of having the aerodynamic loads applied normal to the structure can be resolved by updating the orientation of the aerodynamic panels to match the deformation of the wing. This allows the lift force to act as a follower force, as it follows the deformation of the wing.

32 Case Study

A Bombardier Aircraft platform is used for the purposes of this paper. As a detailed 3D Global Finite Element Model (GFEM) of an aircraft would be very computationally expensive in an iterative aeroelastic analysis, a stick model of the aircraft is used, as shown in Fig. 2.

A stick model is a reduced order model represented by a series of beam elements extending along the aircraft elastic axis that resembles the overall structural behavior of its 3D GFEM counterpart. There are several stick model development methodologies available in the literature [15, 9, 39, 12, 19, 11]. A common stick model development method adopted by the aerospace industry involves the extraction of stick beam equivalent stiffness properties using unitary loading method [39, 12]. This methodology is employed in this paper for the 3D GFEM model order reduction.

Fig. 3 shows a schematic drawing that illustrates the stiffness extraction process of the stick model of a single bay of the 3D GFEM of aircraft wingbox. A wing bay is the segment of the 3D GFEM extending between two consecutive wing stations that is replaced with a single Timoshenko beam element within the stick model reduced order model. Here, the shear centers of the cross-sections at the two ends of a single wing bay are located and a local reference coordinate system is identified at these locations. The shear centre at each subdivision is

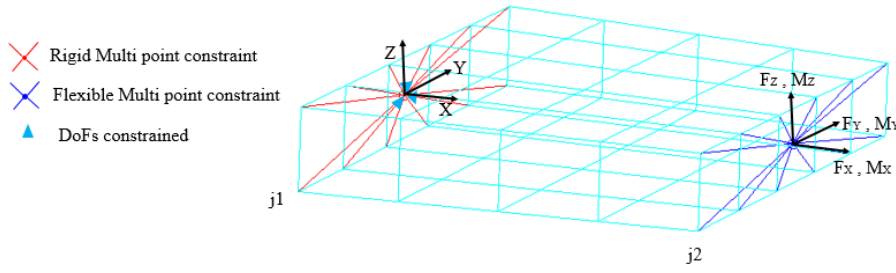


Figure 3: Schematic drawing showing GFEM reduction process to a Stick Model

located by finding the chord-wise point of minimum torsion when a shear load is applied. The defined coordinate system is assumed as a principal coordinate system with its torsional axis extending along the line connecting the predefined shear centers at the ends of the wing bay while the first principal bending axis is assumed along the section airfoil chord line, as shown in Fig. 3. A cantilevered boundary condition is assumed with the inboard end, 1, is fixed. Six load cases involving unit forces and moments are applied at the shear center of the free end, 2, and the stiffness properties for the beam element representing the wing bay are computed as:

$$A_{j1 \rightarrow j2} = \frac{L_{j1 \rightarrow j2}}{E|\delta_{j1 \rightarrow j2}|_x} \quad (29)$$

where $A_{j1 \rightarrow j2}$ is the equivalent cross sectional area, $L_{j1 \rightarrow j2}$ is the bay length, $|\delta_{j1 \rightarrow j2}|_x$ is the axial elongation due to the applied unit load along x-axis and E is the material Young's modulus.

Similarly, the shear factors along the y - and the z - directions, K_y and K_z , respectively, are computed as:

$$(K_y)_{j1 \rightarrow j2} = \frac{L_{j1 \rightarrow j2}}{GA_{j1 \rightarrow j2}|\delta_{j1 \rightarrow j2}|_y} \quad (30)$$

$$(K_z)_{j1 \rightarrow j2} = \frac{L_{j1 \rightarrow j2}}{GA_{j1 \rightarrow j2}|\delta_{j1 \rightarrow j2}|_z} \quad (31)$$

where $|\delta_{j1 \rightarrow j2}|_y$ and $|\delta_{j1 \rightarrow j2}|_z$ denote, respectively, the translational deformation in y- and z- directions due to applied unit forces and G is the material shear modulus.

Moments of inertia of the stick model beam element are computed using the rotational deformations corresponding to the application of unit moments in same manner as described before. The equivalent bending moments of inertia $(I_y)_{j1 \rightarrow j2}$ and $(I_z)_{j1 \rightarrow j2}$, in the y- and z- directions respectively, as well as the equivalent torsional moment of inertia, $(J_x)_{j1 \rightarrow j2}$ in the x-direction, are computed as:

$$(I_y)_{j1 \rightarrow j2} = \frac{L_{j1 \rightarrow j2}}{E|\theta_{j1 \rightarrow j2}|_y} \quad (32)$$

$$(I_z)_{j1 \rightarrow j2} = \frac{L_{j1 \rightarrow j2}}{E|\theta_{j1 \rightarrow j2}|_z} \quad (33)$$

$$(J_x)_{j1 \rightarrow j2} = \frac{L_{j1 \rightarrow j2}}{G|\theta_{j1 \rightarrow j2}|_x} \quad (34)$$

Where $|\theta_{j1 \rightarrow j2}|_x$, $|\theta_{j1 \rightarrow j2}|_y$, and $|\theta_{j1 \rightarrow j2}|_z$ are the angular deformation along x-, y- and z- directions, respectively.

It should be noted that the standard practice in the aerospace industry for aeroelasticity analysis involves the use of lumped mass idealization of the 3D GFEM [14]. The equivalent lumped mass [12] for each aircraft bay can be easily calculated from the aircraft CAD model.

Figure 4: Critical wing loads from wing root to tip normalized with respect to the maximum load from the GFEM model. a) out of plane bending moment, b) out of plane shear force, and c) torsional moment along wing elastic axis.

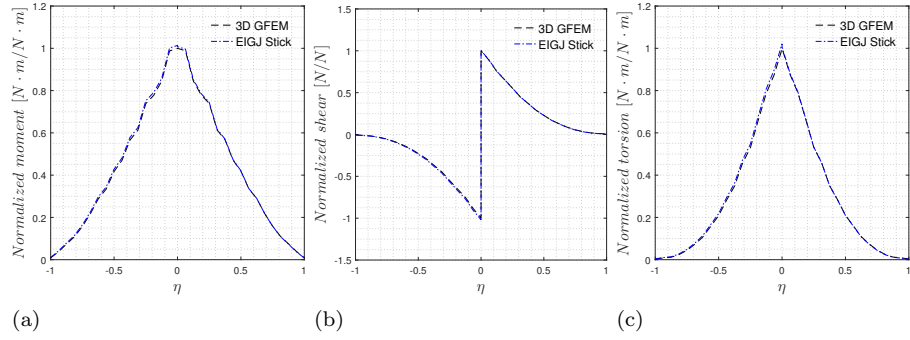


Table 1: Flight conditions for steady flight

Parameter	Value
Mach Number	0.6
Altitude (<i>ft</i>)	29500
Dynamic Pressure (<i>psi</i>)	1.1272
True Airspeed (<i>ft/s</i>)	598.20

The developed stick model was validated by comparing the loads along the wingspan for the aircraft in steady flight using the 3D GFEM model and the reduced stick model, also referred to as the EIGJ stick. The out of plane bending, out of plane shear, and torsional loads are compared along the full wing-span. As can be observed from Figs. 3, there is a very good agreement between the two models, justifying our use of the reduced stick model.

The aerodynamic model of the aircraft requires the inclusion of control surfaces to trim the aircraft at various flight conditions. The control surfaces defined are two ailerons, an elevator, and a rudder. All analyses are run in the steady level flight condition given in Table 1, and the model is free in the plunge and pitch degrees of freedom, and the pitch rate is constrained to zero. The aerodynamic solver, SOL144, poses the problem of trimming the aircraft as a system of equations

As the goal of this study is to document the differences in loads when the aircraft structure is modified, a methodology is needed to create stiffness and mass variations to the structure. In this paper, only the wing elements are modified, leaving the fuselage, horizontal and vertical tails unmodified.

Since the analysis is being performed on an actual aircraft model, the mass and stiffness data points from the sizing optimization of the aircraft, which was provided to us by Bombardier Aerospace, are used to create a relationship between the structural parameters and the resultant mass of each beam element. Following this, each beam element is assumed to have an equivalent rectangular cross-section. The cross-sectional dimensions of the equivalent beam element, namely the width and height, are then parametrized using the given relationships for the beam properties [47], which are used to parametrize the beam properties as functions of their geometry. The relationship between geometry and beam properties are then given by:

$$I_1 = \frac{4ab^3}{3} \quad (35)$$

$$I_2 = \frac{4a^3b}{3} \quad (36)$$

$$J = ab^3 \left[\frac{16}{3} - 3.36 \frac{b}{a} \left(1 - \frac{b^4}{12a^4} \right) \right], a \geq b \quad (37)$$

Equations 35 to 37 allow the beam dimensions to be varied, to create a set of flexibility cases from the baseline structure. The structural mass is obtained using a linear relationship obtained from the design data of the aircraft, which

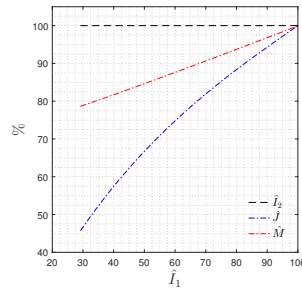


Figure 5: Variation in the in plane stiffness, torsional stiffness, and structural mass of the wing as a function of the out of plane stiffness.

consisted of hundreds of design iterations, where the mass is dependent on the beam dimensional and structural properties. The stiffness data generated can be seen in Fig. 5, where \hat{I}_1 and \hat{I}_2 , are defined as the ratio of the in and out of plane second moment of area, \hat{J} is defined as the ratio of polar moment of area, and \hat{M} is defined as the ratio of the structural weight, with respect to the baseline structural parameters. As the individual beam stiffness along the wing stick model varies, the span-wise distribution of the stiffness is kept constant, and the stiffness parameters of every element along the wings are varied by a scaling factor determined with respect to a single element at the root. This ensures that the only difference in stiffness across all the generated model data is the relative stiffness determined by the aforementioned scaling factor. A program is written in MATLAB to take the reference aircraft and parametrize each of the wing elements by solving Equations 35 to 37 to solve for the equivalent rectangular cross-section. Following this, the dimensions of the equivalent beam cross-section, namely the width and height, are varied to create a new flexible model of the aircraft. The equivalent beam width and height are varied such that the range of out of plane stiffness, I_1 , is changed from 30% to 100% of the reference beam stiffness, and the in plane stiffness, I_2 , remains unchanged. The torsional stiffness, J , is calculated using Eqn. 37. The parametrized model properties are then written into the Nastran beam format, and the Modified Iterative Method is used to determine the loads.

As such, for the purposes of this paper, the out of plane stiffness of the wing is varied from the baseline of 100%, to 30% of the baseline, representing a 21% reduction in weight, \hat{M} . The lower end of the defined range, 30%, was selected by observing the stability of the iterative system. For more flexible variants of the aircraft, it was observed that the aircraft was far too flexible to support itself in steady flight resulting in a high occurrence of numerical convergence issues.

33 Limitations

While the proposed method has significant advantages over the linear Nastran SOL144, it has some limitations which need to be considered when interpreting the results from the method. The first limitation is related to the aerodynamics loads calculation. As the method used to calculate the aerodynamic loads on the aircraft uses Nastran SOL144, the aerodynamics are calculated using linearized potential theory. [35]. As a result, the loads obtained when local wing twist angles are close to stall may not be representative of the physical loads exerted on the aircraft structure. The second limitation of the proposed method, is that it is only applicable to static aeroelastic loads calculation. Despite aeroelasticity inherently being a dynamic process, inertial effects are ignored as the process can be deemed quasi-static, due to the slow moving nature of the flight conditions studied.

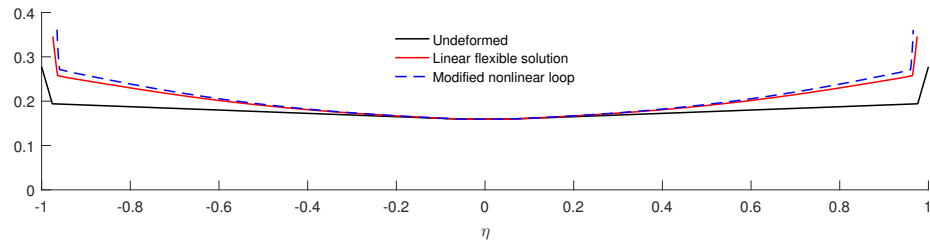


Figure 6: Undeformed and deformed (scaled x 3) structural mesh

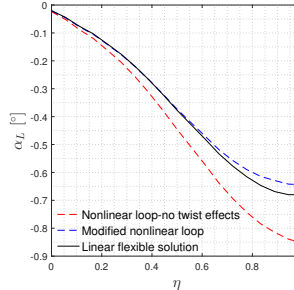


Figure 7: Local angle of attack, α_L , along wingspan

4 Results

4.1 Steady flight conditions

In this section, critical wing loads from the nonlinear methodology, with and without the effect of wing twist, are presented for the relatively stiff baseline aircraft stick model. Results for out of plane bending, out of plane shear, and wing torsional loads along the wing span are presented. Figure 6 depicts the wing displacements under steady flight conditions for the linear and modified nonlinear methods, where η is the normalized position along the wing-span. The displacements have been scaled by a factor of three to help visualize them more clearly.

The results for the out of plane bending moment, shear, and torsion along the wing are presented below in Fig. 9. The loads from the nonlinear loop without twist effects, shown in Fig. 9(a) and 9(b), are significantly affected by the inclusion of geometrically nonlinear effects. This results in the root out of plane bending moment and shear forces being 12% and 7% higher than the loads calculated using linear aeroelastic methods, respectively. The inclusion of wing twisting effects into the loads predicted by the nonlinear methodology brings the difference in out of plane shear and bending moment to less than 2% along the entire wingspan. The root torque, shown in Fig. 9(c), is 2% and 3% higher than the loads obtained from the linear method. The change in loads between the two nonlinear methodologies is attributed to the change in the lift distribution across the wingspan as the effects of downwash are taken into consideration. As a way to validate the modified nonlinear methodology, a nonlinear aeroelastic analysis was run using ASWING [13]. ASWING, developed by Mark Drela at

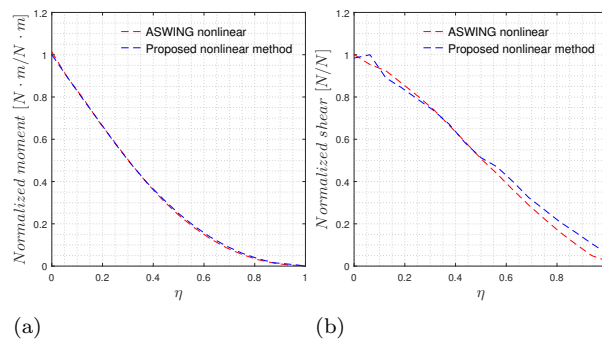


Figure 8: Comparison of a) out of plane bending moment, and b) out of plane shear, between the proposed nonlinear methodology and ASWING [13].

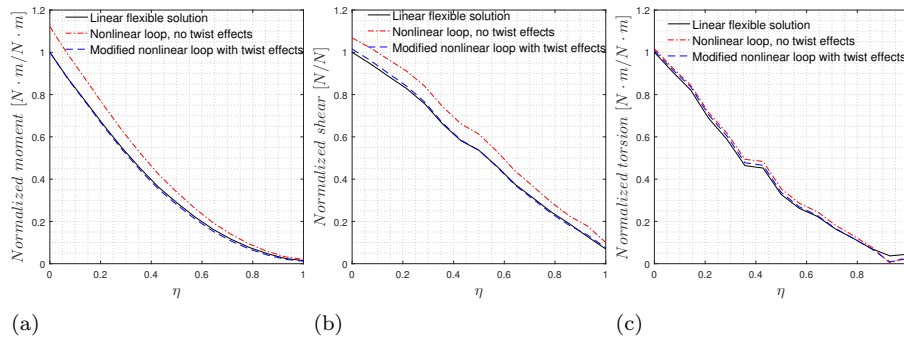


Figure 9: Critical wing loads from wing root to tip normalized with respect to the maximum corresponding linear load. a) out of plane bending moment, b) out of plane shear force, and c) torsional moment along wing elastic axis.

the Massachusetts Institute of Technology, Massachusetts, USA, is a program for the prediction of static and quasi-static loads and deformations of aircraft with flexible surfaces and fuselage beams where fully nonlinear Bernoulli-Euler beam representation is used for all the surface and airframe structures. The baseline airframe was converted to the ASWING format, and the analysis was run under the same flight conditions provided in Table 1. The results, shown in Figure 8, demonstrate a good agreement between the two methods, benchmarking the methodology developed in this paper. Overall, the modified nonlinear methodology results are in agreement with the linear loads for the baseline aircraft stick, which is considered to be relatively stiff. The difference in the loads between the nonlinear methodologies are significant as the out of plane loads calculated by the modified nonlinear methodology are lower than the unmodified loop. This is a result of the change in angle of attack along the outer edges of the wingspan, as shown in Fig. 7, which is not considered in the original modified loop presented. As such, the rest of the results will be presented using the modified nonlinear methodology which includes twist effects.

42 Variation of root angle of attack

The following results are presented as the root angle of attack, α_0 , for the aircraft wing is increased linearly from 0 to 10 degrees. The angle of attack is changed by using a Direct Matrix Input to change the downwash angle at each of the aerodynamic panels of the wing to implement the change in α_0 . The effect of geometric nonlinearity on the out of plane loads can be seen to increase with the angle of attack. Figure 10 shows the variation in the critical wing loads, namely the out of plane bending, out of plane shear, and torsion at the wing root, as the angle of attack increases.

With a root angle of attack of 0 degrees, the out of plane loads along the wing are very close to values obtained from the linear method. This is due to the fact that the aircraft is relatively stiff. As α_0 increases, the loads obtained from both solutions increase, but the loads from the nonlinear solution do not increase as much as the linear loads, indicating that the inclusion of the effect of geometric nonlinearities has the effect of underestimating the loads at high root angles of attack. This is due to the fact that the lift produced by the outboard section of the wing reduces with the increased deformation, resulting in reduced out of plane moment and shear force.

43 Parametric variation of equivalent beam dimensions

43.1 Effect on static aeroelastic loads

As shown in [25], the stiffness of the overall structure has a significant effect on the difference in the loads obtained through classical linear methods as well as nonlinear methods. However, the effect of changes to the individual structural parameters would give a more in depth look into the loads differences due to nonlinearities. The results presented in this section investigate the effects of

Figure 10: Critical wing root loads, normalized with respect to the maximum linear load, with increasing linear load, with increasing root angle of attack, α_0 , for the modified nonlinear loop. a) out of plane bending moment, b) out of plane shear force, and c) torsional moment along wing elastic axis.

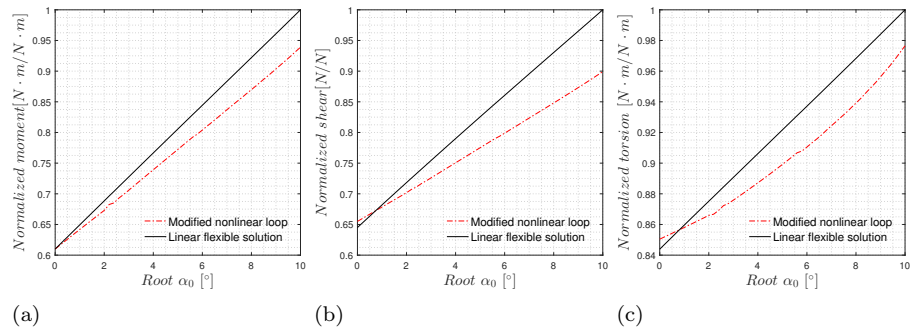
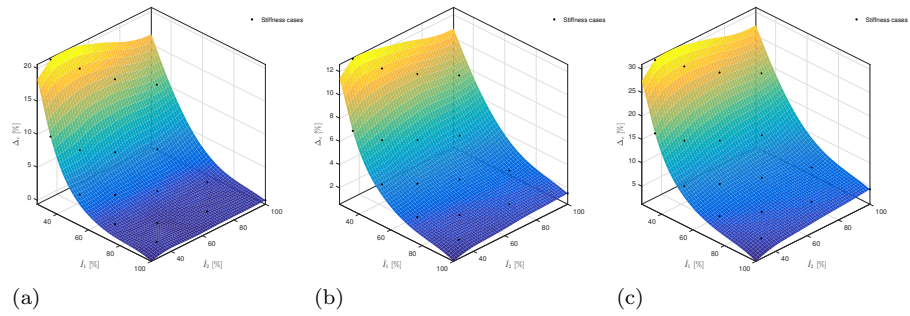


Figure 11: Increase in nonlinear a) out of plane bending moment, b) out of plane shear force, and c) torsional moment at the wing root, Δ_e , compared to the corresponding linear load, with parametric variations of in and out of plane stiffness, \hat{I}_1 and \hat{I}_2



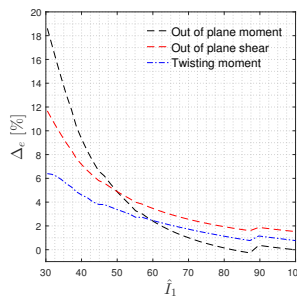
varying the individual beam parameters on the significance of the nonlinearities using the modified nonlinear loop.

The most significant factor observed to affect the nonlinearities is the variation of the flexural stiffness in the out of plane direction. This can be seen very clearly in Fig. 11, where the increase in loads due to the inclusion of nonlinear effects can be seen to be only slightly affected by changes in the in plane stiffness of the wing. As such, the following analyses focus only on the variation of the out of plane stiffness, \hat{I}_1 , keeping \hat{I}_2 at the original reference value of 100%. Figure 12 shows the percentage increase in the root loads, when nonlinearities are considered, Δ_e , over the linear solution for the out of plane bending moment, shear force, and root twisting moment. The percentage increase in wing tip deflection due to the nonlinear solver, Δ_{utip} , is shown in Figure 13.

As shown in Fig. 12, the out of plane bending moment and shear force at the wing root are highly dependent on the out of plane flexural stiffness, resulting in up to a 19% increase in the out of plane bending moment and a 12% increase in the out of plane shear force when the flexural stiffnesses are both reduced to 30% of the original value, while the torsional moment is 6% higher.

The acceptable margin of error for this specific aircraft platform are 1%, 10%, 6% and 10%, for the out of plane bending moment, out of plane shear force,

Figure 12: Nonlinear increase in root loads, Δ_e , with variations of the out of plane stiffness.



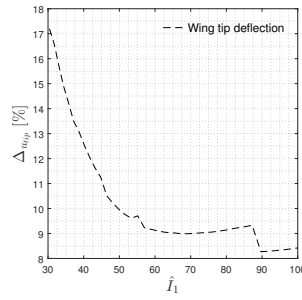


Figure 13: Nonlinear increase in wing tip vertical deflection, Δ_{utip} , with variations of the out of plane stiffness.

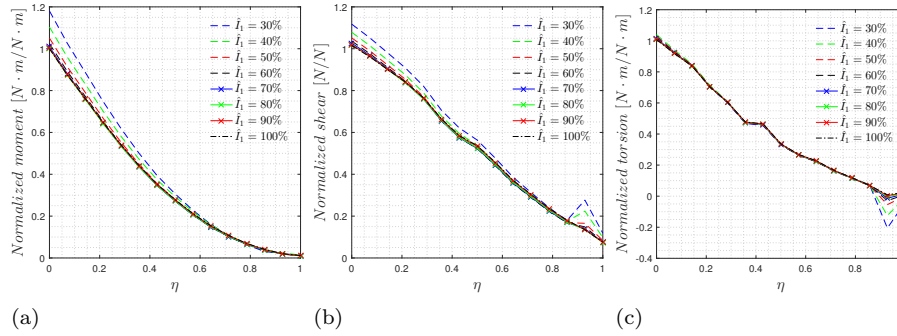


Figure 14: Variation of the increment in loads along the wingspan due to nonlinearity. Critical wing loads plotted here are a) out of plane bending moment, b) out of plane shear force, and c) torsional moment along wing elastic axis.

wing torsional moment, and wingtip deflection respectively. For this airframe, it is observed that the out of plane bending moment exceeds the acceptable load discrepancy criteria when the relative out of plane stiffness, \hat{I}_1 , is lower than 70% of the reference airframe. The threshold at which our allowable margin for the out of plane shear at the root is exceeded, is much lower, with \hat{I}_1 around 35%, while the wing tip deformation threshold is crossed for \hat{I}_1 values below 50%.

Figure 14 shows the wing loads normalized with respect to the root load for the baseline stiffness case, $\hat{I}_1 = 100\%$. It is observed that the loads along the wingspan, vary uniformly when the out of plane flexural stiffness \hat{I}_1 is varied without changing \hat{I}_2 or \hat{J} , with the exception of the out of plane shear and torsional moment at the aileron. This is as a result of the loads exerted by the aileron becoming proportionally more significant to the wing loads as the overall magnitude of the loads decrease with reducing mass. This can be seen in Figure 17(c), which shows the aileron deflection, δ_{ail} , from both linear and nonlinear methodologies. Figures 15 and 16 show the nonlinear and linear critical wing loads along the wing span respectively. The loads are normalized with respect to the linear wing root loads for the 100% stiffness baseline. It can be seen that as the structure of the aircraft is made more flexible, the magnitude of the loads reduces due to the corresponding reduction in mass. However, this reduction is less apparent in the nonlinear case due to the effects of large deformations.

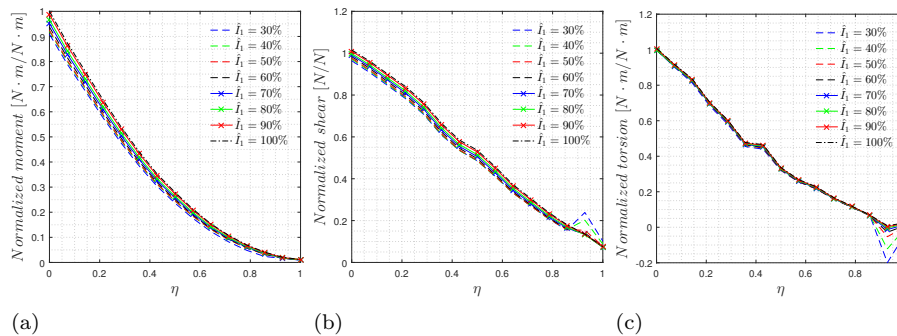


Figure 15: Variation of critical loads along the wing span obtained from the nonlinear iterative method, as the stiffness of the wing is reduced from 100% to 30% of the original values.

Figure 16: Variation of critical loads along the wing span obtained from the linear SOL144, as the stiffness of the wing is reduced from 100% to 30% of the original values.

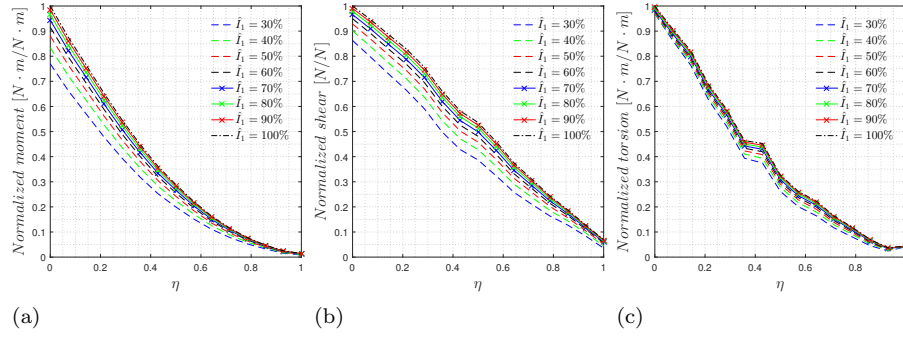
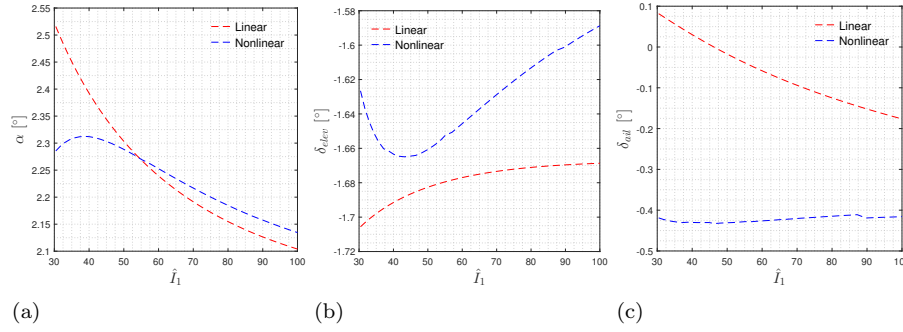


Figure 17: Variation of a) Angle of attack, α , b) elevator deflection, δ_{elev} , and, c) Aileron deflection, δ_{ail} , with variations in the out of plane stiffness, \hat{I}_1 .



43.2 Effect on aircraft trimmed configuration

The change in the deformed structure has a significant effect on the trimming configuration of the aircraft, which can be observed in the change in trimmed angle of attack and elevator deflection. Figures 17 plots the trends of the aircraft trim variables as the flexibility increases. The angle of attack, elevator deflection, and aileron deflection, are shown for both the linear and nonlinear methods used. Of interest to note are the angle of attack and elevator deflection plots, shown in Figures 17(a), 17(b), which show a local change in behaviour at stiffnesses below 50% of the original structure. The aileron deflection remains relatively constant when the nonlinear methodology is used. However, the aileron deflection does induce significant torsional and shear loads in the nonlinear method, as discussed in the previous section, and shown in Figure 14.

5 Conclusions

In this paper, the use of a geometrically nonlinear methodology to calculate static aeroelastic loads results in a significant increase in the out of plane loads for a very flexible airframe. The difference in loads for the stiff baseline aircraft are reasonably close and within 2% of the linear values, but the differences increase as the flexibility of the structure increases. The main driving factor causing the differences is the change in deformed aircraft configuration due to the effects of geometric nonlinearities. The inclusion of wing twist effects into the nonlinear solution can be seen to increase the fidelity of the loads calculated by the nonlinear methodology, and also has a significant impact on the out of plane bending and shear forces experienced at the wing root. Torsional moment was found to be up to 3% higher at the root when nonlinear effects were considered. The variation between the loads from a nonlinear loop and a linear aeroelastic methodology as the root angle of attack was studied. The effects of geometric nonlinearities were found to have a significant impact on the calculation of the critical wing root loads, namely the out of plane bending moment, out of plane shear, and torsional moment. The linear method over predicts the out of plane bending, out of plane shear forces and torsional moment at the root at higher

root angles of attack.

The variation of the structural flexibility parameters has a significant effect on both the resultant loads as well as the final trimmed configuration, however, the primary driving factor here is the out of plane flexural stiffness. A 70% reduction in both the in and out of plane flexural stiffness resulted in the linear solution under predicting the out of plane moment, shear, and wing torque by 19%, 12% and 6% respectively, while the wingtip deflection was 17% higher. It was also determined, for this specific aircraft platform, that the threshold for considering nonlinearities occurs at a 30% reduction in out of plane bending stiffness which corresponds to a 1% difference in loads obtained from linear and nonlinear methodologies. The trimmed configuration of the aircraft was found to have significant changes, especially in the trimmed angle of attack, due to changes in the lift distribution along the wing. Given the modern approach towards more flexible aircraft, it may be possible to use the results from this paper to determine the feasibility of using either a linear or nonlinear aeroelastic methodology for the calculation of aircraft loads when rapid design optimization changes may change the structure and bring about significant geometrically nonlinear effects.

Acknowledgments

The research presented in this paper is funded by Bombardier Aerospace, the Consortium for Aerospace Research and Innovation in Canada (CARIC) and by Mitacs Canada.

References

- [1] A Abbas, J De Vicente, and E Valero. Aerodynamic technologies to improve aircraft performance. *Aerospace Science and Technology*, 28(1):100–132, 2013.
- [2] Frederico Afonso, José Vale, Éder Oliveira, Fernando Lau, and Afzal Suleman. A review on non-linear aeroelasticity of high aspect-ratio wings. *Progress in Aerospace Sciences*, 2017.
- [3] Edward Albano and William P Rodden. A doublet-lattice method for calculating lift distributions on oscillating surfaces in subsonic flows. *AIAA journal*, 7(2):279–285, 1969.
- [4] John David Anderson Jr. *Fundamentals of aerodynamics*. Tata McGraw-Hill Education, 2010.
- [5] Klaus-Jürgen Bathe, Ekkehard Ramm, and Edward L Wilson. Finite element formulations for large deformation dynamic analysis. *International Journal for Numerical Methods in Engineering*, 9(2):353–386, 1975.
- [6] O. A Bauchau and C. H. Hong. Large displacement analysis of naturally curved and twisted composite beams. *AIAA journal*, 25(11):1469–1475, 1987.
- [7] O. A. Bauchau and C. H. Hong. Nonlinear composite beam theory. *ASME, Transactions, Journal of Applied Mechanics*, 55:156–163, 1988.
- [8] Ted Belytschko, Wing Kam Liu, Brian Moran, and Khalil Elkhodary. *Nonlinear finite elements for continua and structures*. John wiley & sons, 2013.
- [9] G Bindolino, G Ghiringhelli, S Ricci, and M Terraneo. Multilevel structural optimization for preliminary wing-box weight estimation. *Journal of Aircraft*, 47(2):475–489, 2010.

- [10] Javier Bonet and Richard D Wood. Nonlinear continuum mechanics for finite element analysis. Cambridge university press, 1997.
- [11] R. Cirillo. Detailed and condensed finite element models for dynamic analysis of a business jet aircraft. MS Thesis, Politecnico di Milano, Italy, 2011.
- [12] Guillaume Corriveau and Franck Dervault. Impact of wing box geometrical parameters on stick model prediction accuracy. In 54th AIAA/ASME/ASCE/AHS/ASC Structures, Structural Dynamics, and Materials Conference, page 1810, 2013.
- [13] Mark Drela. Aswing 5.99 technical description. Massachusetts Inst. of Technology, Cambridge, MA, 2015.
- [14] J. Barron E. Bosco, J. Morlier and A. Lucchetti. Influence of mass modelling in dynamic landing simulations. In 10th PEGASUS-AIAA student conference, 2014.
- [15] Mostafa SA Elsayed, Ramin Sedaghati, and Mohammed Abdo. Accurate stick model development for static analysis of complex aircraft wing-box structures. AIAA journal, 47(9):2063–2075, 2009.
- [16] Matija Gams, Igor Planinc, and Miran Saje. The strain-based beam finite elements in multibody dynamics. Journal of sound and vibration, 305(1):194–210, 2007.
- [17] Joseph A Garcia. Numerical investigation of nonlinear aeroelastic effects on flexible high-aspect-ratio wings. Journal of Aircraft, 42(4):1025–1036, 2005.
- [18] David L Greene. Energy-efficiency improvement potential of commercial aircraft. Annual Review of Energy and the Environment, 17(1):537–573, 1992.
- [19] Mostafa Hashemi-Kia and Mostafa Toossi. Development and application of a technique for reducing airframe finite element models for dynamics analysis. 1990.
- [20] G.A. Hegemier and S Nair. A nonlinear dynamical theory for heterogeneous, anisotropic, elastic rods. AIAA Journal, 15(1):8–15, 1977.
- [21] Dewey H Hodges. A mixed variational formulation based on exact intrinsic equations for dynamics of moving beams. International journal of solids and structures, 26(11):1253–1273, 1990.
- [22] Dewey H Hodges. Geometrically exact, intrinsic theory for dynamics of curved and twisted anisotropic beams. AIAA journal, 41(6):1131–1137, 2003.
- [23] Dewey H Hodges. Erratum: Geometrically exact, intrinsic theory for dynamics of curved and twisted anisotropic beams. AIAA journal, 47(5):1308–1309, 2009.
- [24] Dewey H Hodges, Wenbin Yu, and Mayuresh J Patil. Geometrically-exact, intrinsic theory for dynamics of moving composite plates. International Journal of Solids and Structures, 46(10):2036–2042, 2009.
- [25] Chris Howcroft, Dario Calderon, Luke Lambert, Michele Castellani, Jonathan E Cooper, Mark H Lowenberg, and Simon Neild. Aeroelastic modelling of highly flexible wings. In 15th Dynamics Specialists Conference, page 1798, 2016.

- [26] Sang H. Lee. MSC/NASTRAN Nonlinear Analysis Handbook. MSC Software Corporation, 1992.
- [27] Eli Livne and Terrence A Weisshaar. Aeroelasticity of nonconventional airplane configurations-past and future. Journal of Aircraft, 40(6):1047–1065, 2003.
- [28] Augustus Edward Hough Love. A treatise on the mathematical theory of elasticity. Cambridge university press, 1982.
- [29] Kenneth W McAlister, O Lambert, and D Petot. Application of the onera model of dynamic stall. NASA Technical Paper 2399 AVSCOM Technical Report 84-A-3, NASA Ames Research Center, 1984.
- [30] J Oliver and E Onate. A total lagrangian formulation for the geometrically nonlinear analysis of structures using finite elements. part i. two-dimensional problems: Shell and plate structures. International Journal for Numerical Methods in Engineering, 20(12):2253–2281, 1984.
- [31] Mayuresh J Patil and Dewey H Hodges. Flight dynamics of highly flexible flying wings. Journal of Aircraft, 43(6):1790–1798, 2006.
- [32] Mayuresh J Patil, Dewey H Hodges, and Carlos ES Cesnik. Characterizing the effects of geometrical nonlinearities on aeroelastic behavior of high-aspect ratio wings. In Proceedings of the International Forum on Aeroelasticity and Structural Dynamics, pages 501–510, June 22-25 1999.
- [33] Mayuresh J Patil, Dewey H Hodges, and Carlos ES Cesnik. Nonlinear aeroelasticity and flight dynamics of high-altitude long-endurance aircraft. Journal of Aircraft, 38(1):88–94, 2001.
- [34] Eric Reissner. On one-dimensional large-displacement finite-strain beam theory. Studies in applied mathematics, 52(2):87–95, 1973.
- [35] William P Rodden and Erwin H Johnson. MSC/NASTRAN aeroelastic analysis: user's guide; Version 68. MacNeal-Schwendler Corporation, 1994.
- [36] Ha-Sang Ryu and Hyo-Chol Sin. Curved beam elements based on strain fields. International Journal for Numerical Methods in Biomedical Engineering, 12(11):767–773, 1996.
- [37] Muthukrishnan Sathyamoorthy. Nonlinear analysis of structures, volume 8. CRC Press, 1997.
- [38] Christopher M Shearer and Carlos ES Cesnik. Nonlinear flight dynamics of very flexible aircraft. Journal of Aircraft, 44(5):1528–1545, 2007.
- [39] Ashok K Singh and CW Nichols. Derivation of an equivalent beam model from a structural finite element model. In Proceedings of the MSC 1988 World Users Conference, 1988.
- [40] Weihua Su and Carlos ES Cesnik. Strain-based geometrically nonlinear beam formulation for modeling very flexible aircraft. International Journal of Solids and Structures, 48(16):2349–2360, 2011.
- [41] Deman Tang and Earl H Dowell. Experimental and theoretical study on aeroelastic response of high-aspect-ratio wings. AIAA journal, 39(8):1430–1441, 2001.
- [42] Marthinus C Van Schoor and Andreas H von Flotow. Aeroelastic characteristics of a highly flexible aircraft. Journal of Aircraft, 27(10):901–908, 1990.

- [43] HT Vivian and LV Andrew. Unsteady aerodynamics for advanced configurations. part i. application of the subsonic kernel function to nonplanar lifting surfaces. Technical report, NORTH AMERICAN AVIATION INC DOWNEY CA SPACE AND INFORMATION SYSTEMS DIV, 1965.
- [44] Jinwu Xiang, Yongju Yan, and Daochun Li. Recent advance in nonlinear aeroelastic analysis and control of the aircraft. Chinese Journal of Aeronautics, 27(1):12–22, 2014.
- [45] Chang Chuan Xie, Jia Zhen Leng, and Chao Yang. Geometrical nonlinear aeroelastic stability analysis of a composite high-aspect-ratio wing. Shock and Vibration, 15(3, 4):325–333, 2008.
- [46] Chang Chuan Xie and Chao Yang. Linearization method of nonlinear aeroelastic stability for complete aircraft with high-aspect-ratio wings. Science China Technological Sciences, 54(2):403–411, 2011.
- [47] Warren Clarence Young and Richard Gordon Budynas. Roark’s formulas for stress and strain, volume 7. McGraw-Hill New York, 2002.
- [48] Olek C Zienkiewicz and Robert L Taylor. The finite element method for solid and structural mechanics. Butterworth-heinemann, 2005.
- [49] Dejan Zupan and Miran Saje. Finite-element formulation of geometrically exact three-dimensional beam theories based on interpolation of strain measures. Computer Methods in Applied Mechanics and Engineering, 192(49):5209–5248, 2003.